Free-standing microporous paper-like graphene films with electrodeposited PPy coatings as electrodes for supercapacitors

Lili Jiang · Xiong Lu · Jielong Xu · Yingqi Chen · Guojiang Wan · Yonghui Ding

Abstract Free-standing microporous paper-like graphene films with electrodeposited polypyrrole (PPy) coatings were prepared. The microporous structures were produced by employing PS microspheres as sacrificial templates. PPy was coated on the films using an electrochemical deposition process to further improve the performance of these graphene electrode materials. The electrochemical performance of PPy coated microporous graphene films is evaluated and compared with solid graphene films. The results reveal that the incorporation of PPy and microporous structures significantly improve the electrochemical performance of graphene based electrodes for supercapacitors. Microporous films have higher capacitance than their solid counterparts although they have slightly lower conductivity, which reveals that microporous structures play an important role in the electrochemical performance of the electrode materials. The PPy coated microporous graphene films have the better electrochemical performance than uncoated counterparts, which indicates that PPy coatings have significant effects on graphene based electrodes. This in-depth research on free-standing microporous paper-like graphene with electrodeposited PPy coatings provides a new route to combine the advantages of both graphene and PPy so as to produce high performance electrodes for supercapacitors.

L. Jiang · X. Lu (✉) · J. Xu · Y. Chen · G. Wan
Key Lab of Advanced Technologies of Materials, Ministry of Education, School of Materials Science and Engineering, Southwest Jiaotong University, Chengdu 610031, Sichuan, China
e-mail: luxiong_2004@163.com

Y. Ding
Department of Mechanical Engineering, Hong Kong University of Science and Technology, Kowloon, Hong Kong, China

1 Introduction

Supercapacitors are kinds of energy storage applications that can provide higher power density and higher energy density than conventional electrical devices, and have been widely used in various fields, such as intelligent instruments, toys, automotive electronics and solar energy [1–3]. Supercapacitors are divided into three families according to different electrode materials, including electrical double-layer capacitors (EDLC), pseudocapacitors, and hybrid capacitors. The high performance of supercapacitors is largely dependent on the electrode materials. Graphene has been recognized as a promising candidate electrode material because it has intriguing properties such as high conductivity, great mechanical strength and thermal conductivity [4, 5]. Liu et al. [6] used a freeze-drying method to produce flexible and foldable graphene paper, which shows significantly improved performance compared with available carbon materials. Wang et al. [7] used a vacuum filtration method to develop flexible graphene paper, which was used as EDLC electrodes for supercapacitors and exhibits excellent electrochemical performance.

Recently, graphene with micro/nano porous structures has been developed as electrode materials to further improve the performance of supercapacitors. For example, Lee et al. [8] and Zhi et al. [9] used chemical vapor deposition process to deposit graphene on Ni foams to produce three dimensional porous graphene, which was applied as electrodes for supercapacitors and proved to
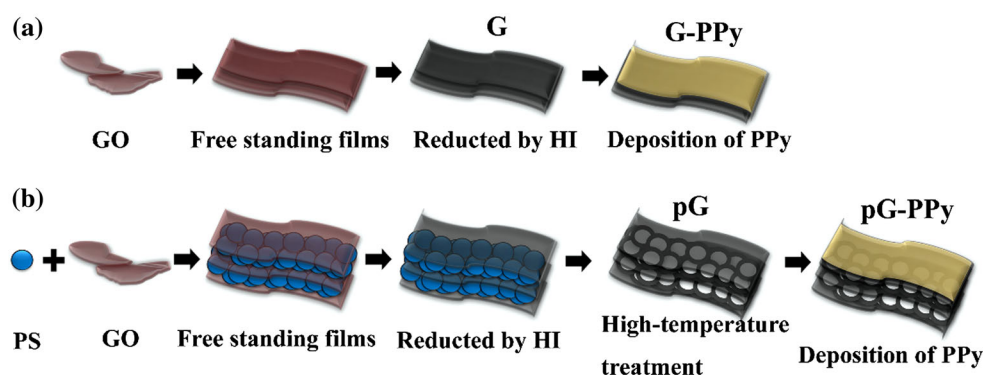
Fig. 1 a Schematics of the fabrication process of free-standing paper-like PPy coated G films, **b** the fabrication process of microporous PPy coated G films

have good electrochemical performance. This process involves tedious Ni foam etching process. Kim et al. [10] used microwave expansion and KOH activation methods to fabricate a highly porous graphene with hierarchical porous structures. Hu et al. [11] also use a simple solvent treatment process to produce mesoporous graphene with three dimensional structures. However, the porous structure through these methods was uncontrollable. The uncontrollable and erose structure may hamper the analysis and understanding of the effect of porous structure on ion diffusion and storage. Hence, polystyrene (PS) microspheres with their characteristics of uniform size and easily removal were newly recognized as suitable sacrificial templates in porous graphene fabrication. Choi et al. [12] employed PS microspheres as sacrificial templates to produce microporous graphene, and they demonstrated that the microporous graphene has a high performance when it is used as the electrode for supercapacitors.

Polypyrrole (PPy) as one conducting polymer has been used in supercapacitors because of its high electrical conductivity and good electrochemical stability. PPy can store charges based on its electrical double layer property and rapid faradic charge transfer ability [13, 14]. The combination of PPy and graphene has attracted a great deal of attention for the compensation of conductivity and improvement of mechanical properties of PPy. Normally, there are two processes to produce PPy, including in situ oxidative polymerization and electrooxidation. De Oliveira et al. [15] used a process of in situ oxidative polymerization of PPy on functionalized graphene sheets to produce high-quality graphene–PPy composites as electrode materials for supercapacitors. Electrooxidation process is another commonly used method to produce PPy, which is popular for its facile, low-cost and environmental friendly characteristics. Chang et al. [16] used electrooxidation process to obtain graphene oxide and PPy composites as electrode for supercapacitors, which has been demonstrated to have good electrochemical performance. Liu et al. [17]

also used electrochemical deposition process to produce sulfonated graphene and PPy composites as electrodes.

In this study, free-standing microporous paper-like graphene films with electrodeposited PPy coatings are prepared, as shown in Fig. 1. First, a self-assemble process is used to prepare free-standing, paper-like graphene films with microporous structures, which is produced by employing PS microspheres as sacrificial templates. Secondly, PPy is directly deposited on graphene films using electrochemical deposition process to further improve the performance of these graphene electrode materials. Finally, the electrochemical performance of PPy coated microporous graphene films is evaluated.

2 Materials and methods

2.1 Synthesis of graphene oxide (GO)

GO was synthesized using a modified Hummer's method. The detail has been reported in the previous Refs. [18, 19]. Briefly, 10 g of graphite power (diameter <20 μm, Sigma-Aldrich) and 230 ml of H_2SO_4 (98 %) was mixed in a flask and stirred for 2 h. 50 g of $KMnO_4$ was added slowly into the mixture while the temperature was kept at 0 °C. Then the mixture was moved into a water bath and kept at 35 °C for 30 min. Deionization (DI) water was added continuously into the mixture and stirred vigorously. The temperature was increased to 90 °C and maintained for 30 min. Finally, 30 ml of H_2O_2 (30 %) was added into the mixture to end the reaction. The mixture was filtered through a polypropene (PP) Millipore filter (pore size, 0.2 μm), washed with DI water for several times. The production of filtration was dissolved in DI water to obtain raw GO solution. This raw GO solution was further centrifuged at 4,000 rpm for 10 min and supernatant was collected, which is the final homogeneous GO dispersion.
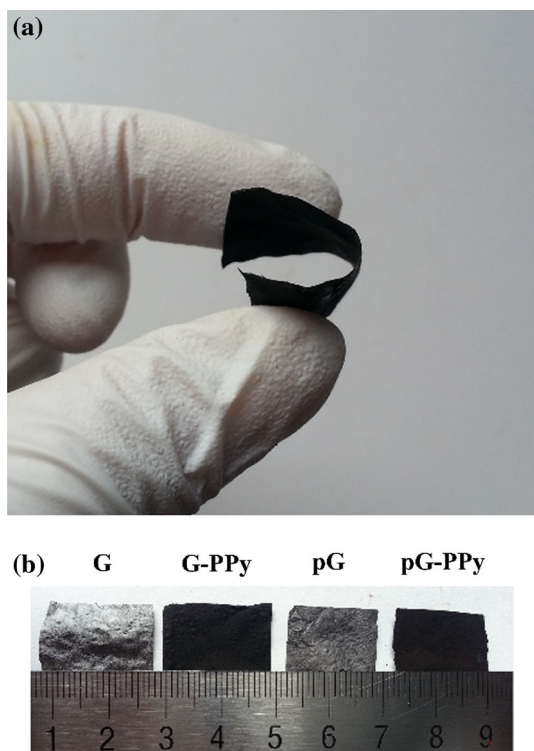
Fig. 2 a Photograph of a paper-like PPy coated solid G film, b photograph of the as-prepared G, G-PPy, pG, pG-PPy films

2.2 Preparation of graphene films

As shown in Fig. 1a, 50 ml of homogeneous GO dispersions (5 mg/ml) were poured into a mould. The solution was then heated under 70 °C till DI water was completely evaporated, and a smooth free standing GO films was obtained. The as-prepared GO films were then reduced by hydriodic acid (HI 57 %) [20]. GO films were immersed in HI acid solution in a sealed cuvette that was placed in a water bath at 80 °C for 2 h. After washed with DI water for several times, the graphene films was produced, named as G.

2.3 Preparation of microporous graphene films

As shown in Fig. 1b, 0.3 g of PS microspheres were mixed with 2.1 ml of DI water and ultrasonic vibrated to obtain a homogeneous PS solution firstly. The detail of synthesis of PS microspheres was described in Supporting Information. Next, 0.024 g of sodium dodecyl sulfate (SDS; Biotech) and 0.024 g of ethanol was added in 2.4 g of PS solution. PS microspheres were tightly ordered and well assembled after the addition of SDS. In the third step, the obtained PS solution was mixed with 50 ml of GO solution (5 mg/ml) to obtain GO-PS films by using the same process as the production of G films. Then, the HI reduction process was
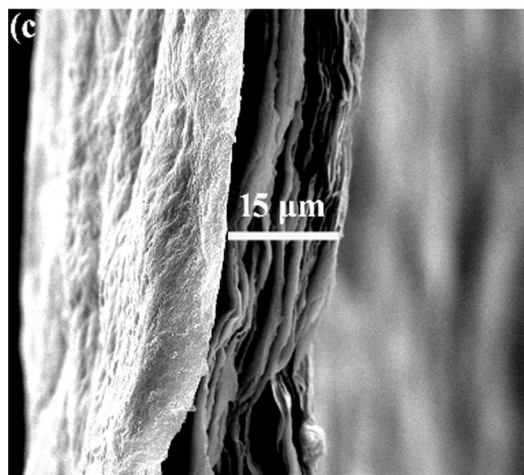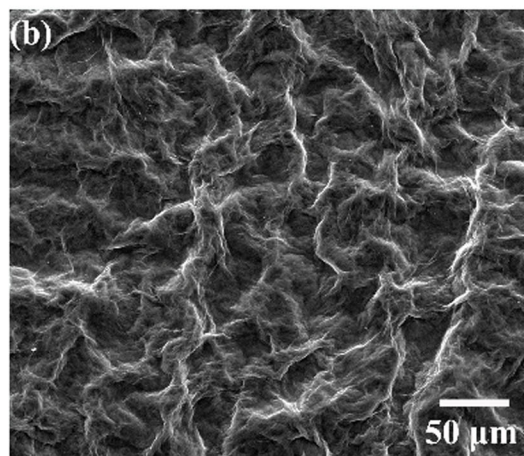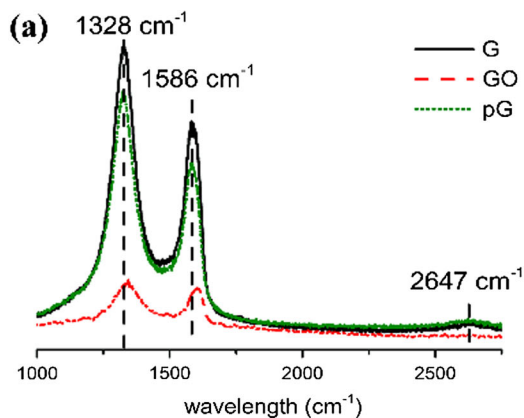

Fig. 3 a Raman spectra of GO, G and pG films, b the morphology of G films, c the cross section of G films

applied to reduce the GO-PS films. Finally, a high temperature treatment was carried out at 500 °C for 2 h to remove the PS microsphere templates so as to obtain microporous G films, named as pG. The porosity of microporous G films was calculated according to Eq. (1)

$$P = \frac{V}{V_0} = \frac{m/\rho}{ST} \qquad (1)$$

Fig. 4 **a** *Top view* of GO-PS composite films, **b** the cross section of GO-PS composite films, **c** G-PS composite films after the reduction of GO by HI, **d** the cross section of G-PS composite films after reduction, **e** pG films after the removal of PS microspheres by high-temperature treatments, **f** the cross section of microporous pG films (the *inset* shows the thickness of microporous G films)
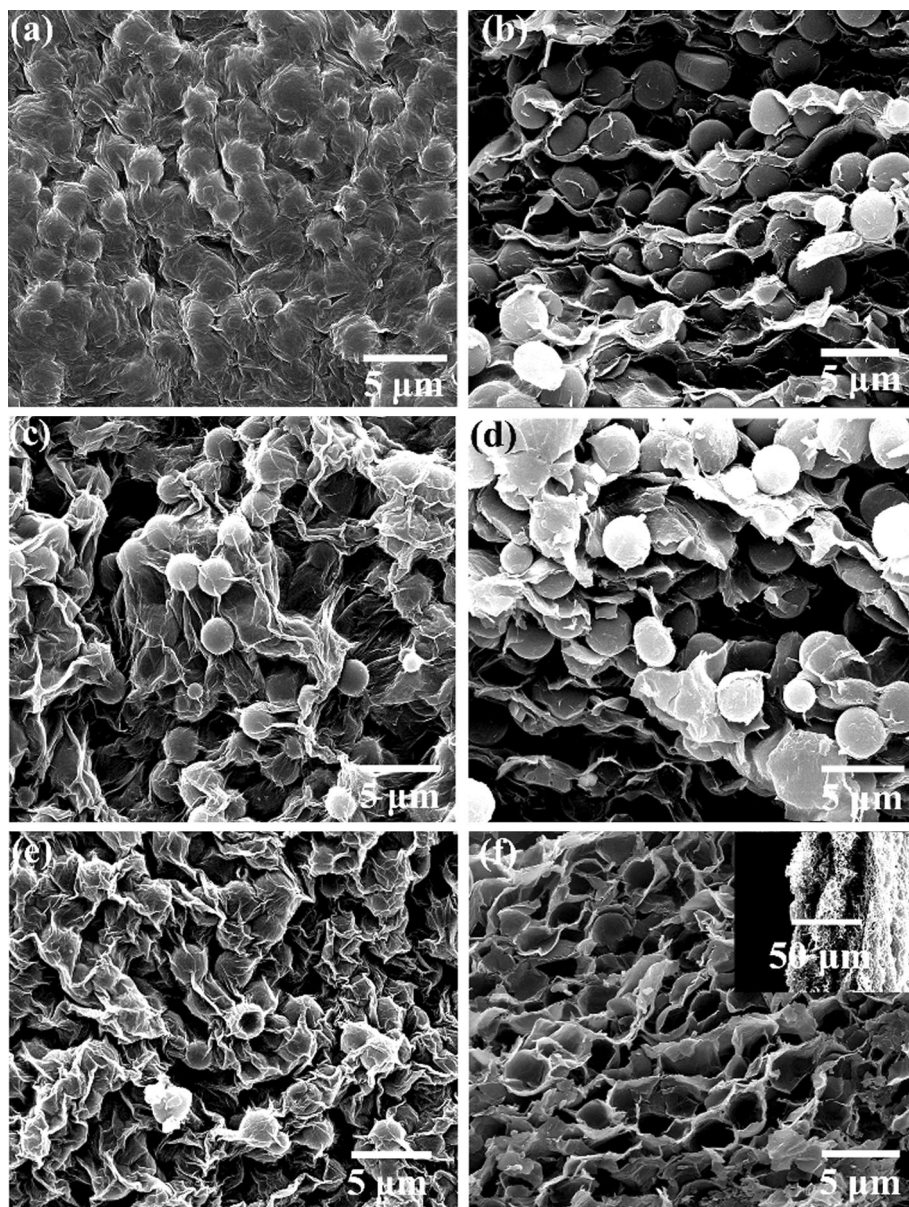
where *V* is the total volume of PS, which was calculated through mass divided by density; V_0, S, and T are the volume, the area and the thickness of the microporous graphene film, respectively.

## 2.4 Electrochemical deposition of PPy

Electrochemical deposition of PPy on graphene films was carried out at room temperature using a potentiostate (CHI600B, CH Instruments, China). The as-prepared G film, a Pt foil and a saturate calomel electrode acted as the working, counter, and reference electrodes, respectively. The potential was set as 1 V. The electrolyte is 2.8 ml of

pyrrole (Sigma-Aldrich) in 200 ml of NaCl solution (0.1 M). During the electrochemical process, the polymerization of pyrrole occurred and PPy coatings were deposited on the surface of G and pG films, which were named as G-PPy and pG-PPy, respectively.

2.5 Characterization methods

A scanning electron microscope (SEM; INSPECT-F, FEI, The Netherlands) was used to analyze the morphology of the films. The Raman spectra were recorded with a Renishaw 2000 Confocal Raman Microprobe (Renishaw Instruments, UK). Fourier transform infrared spectroscopy

Fig. 5 **a** The morphology of G-PPy films, **b** the morphology of pG-PPy films, **c** the cross-sectional view of pG-PPy shows the PPy coatings on the microporous G films, as indicated by the *arrow*, **d** FT-IR spectrum of PPy coatings on G films
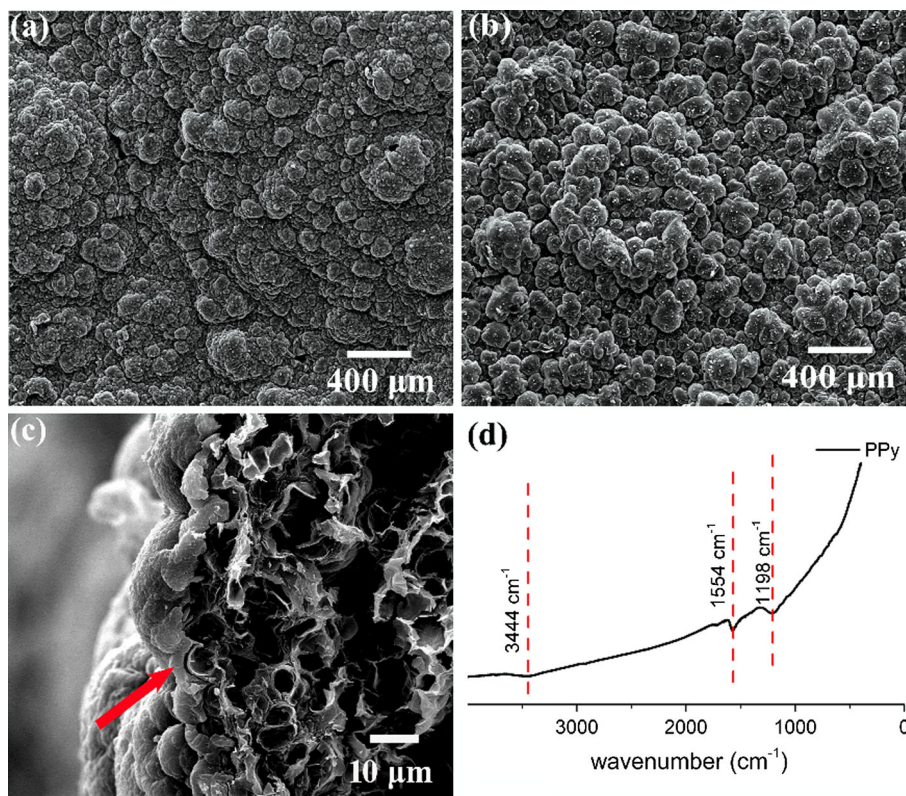
Table 1 Conductivity of the G-based films

Sample	Resistivity (Ω m)
G	$(4.49 \pm 0.07) \times 10^{-4}$
G-PPy	$(1.36 \pm 0.28) \times 10^{-4}$
pG	$(22.53 \pm 2.51) \times 10^{-4}$
pG-PPy	$(6.67 \pm 2.24) \times 10^{-4}$

(FT-IR; Nicolet 5700, Thermo Nicolet, USA) was used to prove the synthesis of PPy and PS. The conductivity of the films was measured by a four-probe resistivity test system (RTS-9, Probes Tech, China).

An electrochemical analytical system (IM6, Zahner elektrik GmbH, Germany) was used for the measurements of electrochemical performance of the films. The cyclic voltammetry (CV) was tested in the potential range from 0 to 1 V in the electrolyte of 1 M H_2SO_4 at room temperature. CV was scanned at the scan rate of 5, 10, 20, and 40 mV s^{-1}. The specific capacitance C_{sp} (F g^{-1}) was calculated by following Eq. (2)

$$C_{sp} = \frac{\int I dV}{v m \Delta V} \tag{2}$$

where I is the current, V is the voltage, ΔV is the width of the voltage window, v is the scan rate, m is the mass of G based electrodes.

The area capacitance C_a (F cm^{-2}) at each scan rate was calculated by following Eq. (3)

$$C_a = \frac{\int I dV}{v A \Delta V} \tag{3}$$

where A is the area of our ultra-thin graphene based electrode.

The galvanostatic charge–discharge measurement was also conducted in the electrolyte of 1 M H_2SO_4. A constant current of 0.2 mA is applied and the potential range is from 0 to 1 V.

The energy density and the power density was calculated according to Eqs. (4) and (5)

$$E = \frac{1}{2} C_a \Delta V^2 \tag{4}$$

$$P = \frac{E}{\Delta t} \tag{5}$$

3 Results and discussion

3.1 Graphene films

Photographs of the graphene based electrode materials in this study are shown in Fig. 2. The Raman spectra proves the success of efficient HI reduction process (Fig. 3a). Two prominent peaks present in the spectrum, namely the D band (1,328 cm^{-1}) and G band (1,586 cm^{-1}). The I_D/I_G
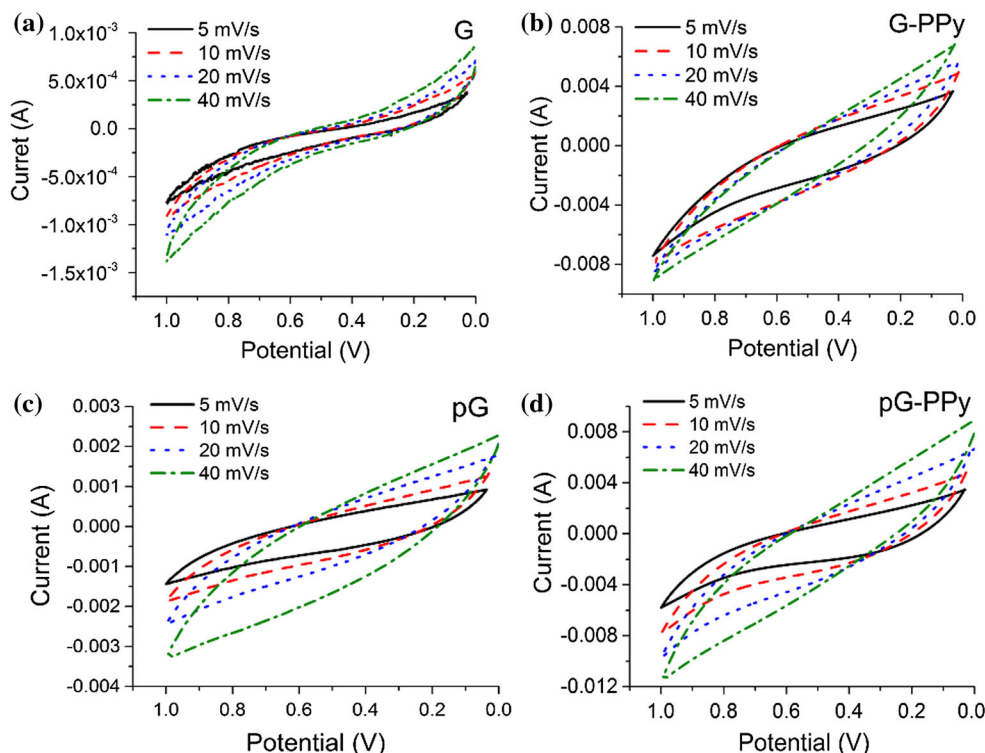
Fig. 6 The CV profiles of various electrodes at a series of scan rates. **a** G, **b** G-PPy, **c** pG, **d** pG-PPy

ratio represents the reciprocal of the average size of crystallite in graphite [19]. I_D/I_G ratio increases after GO is reduced by HI, which proves the conjugated G network is re-established. It is noteworthy that the I_D/I_G ratio of G (1.35) is higher than that of pG (1.33), which could be ascribed to the microporous internal structures of pG that diminish the reduction efficiency during the HI reduction process. The peak at 2,647 cm^{-1} also suggests the restoration of sp^2 carbon in G and pG film [20]. SEM micrograph reveals the typical wrinkle structure of G (Fig. 3b). The thickness of G films is 15 μm, as shown in the cross-sectional view (Fig. 3c). The cross-sectional view of G films also reveals the layer by layer stacking structure of G films. The aggregation and stacking of G sheets could be a limitation to the diffusion of electrolyte and diminish the capacitance performance of the G electrode [21, 22].

3.2 Microporous graphene films

SEM micrograph reveals the morphology and cross-section of microporous G based films at different stages of processing (Fig. 4). Figure 4a, b show the morphology of GO-PS films, which indicates that the PS microspheres uniformly disperse in GO films and pack into multilayers. After reduced by HI, the GO appears a silk-like morphology and the PS microspheres that are wrapped in the nanosheets and can be seen through the silk-like nanosheets (Fig. 4c). The intercalated structure of PS and graphene is well kept after the

reduction process, as revealed by the cross sectional view (Fig. 4d). After the removal of PS by the heat treatment, the spherical and porous structures are generated in the films (Fig. 4e), and the well-defined internal micropores are uniformly distributed in the center of the films (Fig. 4f). The thickness of pG is 50 μm, as shown by the inset in Fig. 4f.

3.3 PPy coated graphene films

The PPy coated G film appears in a deep dark color because the deposited PPy conceals the original metal color of G films (Fig. 2b). The SEM micrograph of G-PPy reveals that the spherical PPy seamlessly covers on the whole G film (Fig. 5a). The surface of pG-PPy is rougher than that of G-PPy (Fig. 5b). The cross-sectional view of pG-PPy proves that PPy is uniformly deposited on pG films and the thickness of PPy is about 2 μm (Fig. 5c). FT-IR spectrum of PPy shows the characteristic peaks of PPy (Fig. 5d). The peak at 3,444 cm^{-1} is due to the N–H stretching of PPy ring. The peak at 1,554 cm^{-1} is assigned to the typical PPy ring vibrations. The peak at 1,198 cm^{-1} corresponds to C–C stretching of G.

3.4 The conductivity and porosity of films

The resistivities of four G-based films are listed in Table 1. The PPy coated films have lower resistivity than the contra groups, which indicates that PPy is very
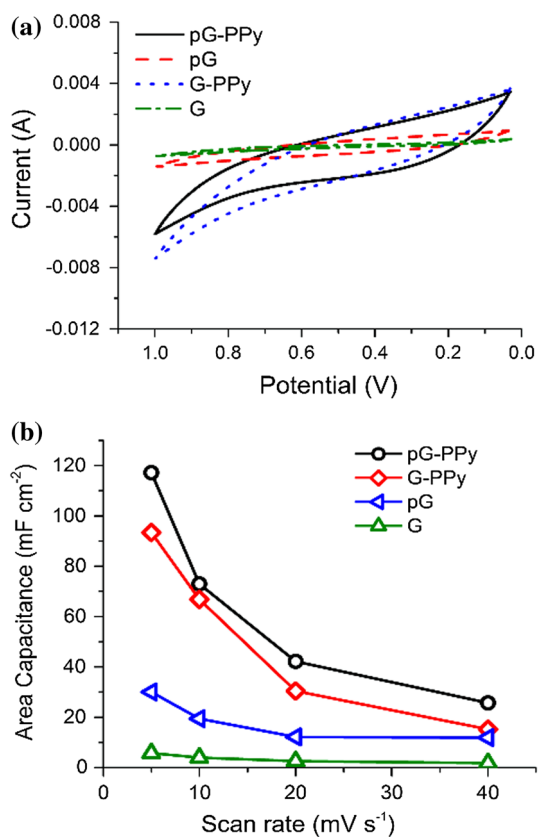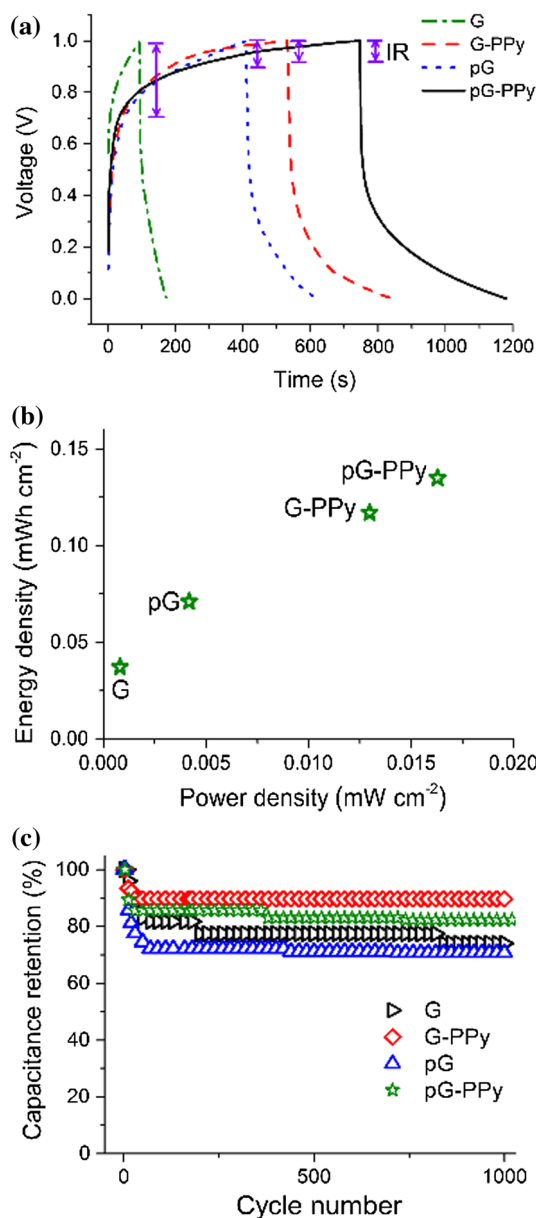
Fig. 7 **a** The CV profiles of four electrodes at the scan rate of 5 mV s^{-1}, **b** capacitive performances of as-prepared electrodes versus scan rates

helpful to improve the conductivity of graphene films. It is also noted that microporous samples have higher resistivity than their counterparts, which might be due to the weak internal connection of the microporous structure of G sheets [23]. The porosity of pG and pG-PPy is 70.9 %.

3.5 Electrochemical performance of electrodes

The typical CV profiles of four electrodes with scan rates from 5 to 40 mV s^{-1} are shown in Fig. 6. The CV profiles of electrode G and pG exhibit a rectangular shape with a series of scan rates (Fig. 6a, c), indicating EDLC behavior of these electrodes. The CV profiles of G-PPy and pG-PPy exhibit a nearly rectangle shape with very slight redox peaks that are caused by the oxidation and reduction of PPy, indicating a pseudocapacitor behavior. These CV profiles keep in shape at a high scan rate although they show an increased leaning angle to the voltage-axis with the increasing scan rate in different levels, which indicates that the electrodes have low equivalent series resistance and ions can fast diffuse between electrolyte and electrodes [9, 24, 25].

Fig. 8 **a** The galvanostatic charging–discharging profiles of the electrodes, **b** the Ragone plot of the electrode, **c** cycle life performance of the electrodes at the current of 0.2 mA

The CV profiles of each sample at the scan rate of 5 mV s^{-1} are compared and the specific capacitance and area capacitance of these graphene based electrodes are estimated based on the CV profiles (Fig. 7a). It reveals that pG-PPy has the highest capacitance and the value reaches at 131.1 F g^{-1} (117.2 F cm^{-2}), which is higher than that of G-PPy (111.2 F g^{-1}, 93.4 F cm^{-2}) and pG (35.9 F g^{-1}, 30.1 F cm^{-2}). G has the lowest capacitive performance of only 8.28 F g^{-1} (5.7 F cm^{-2}). The area capacitive performances versus varied scan rates are presented in Fig. 7b, which reveals that the pG-PPy electrode has the best performance in spite of different scan rates. The decrease of

capacitance of four electrodes along with the increase of scan rate suggests the slow diffusion of ions at high scan rates.

Comparison of PPy coated and bare G films indicates that the capacitance of G films, which has a EDLC behavior, are enhanced by the incorporation of PPy, which has a pseudocapacitor behavior. Moreover, the attachment of PPy on the surface of pG improves the conductivity of G and reduces the diffusion and migration length of electron, which results in a more effective utilization of electrons and further improve the capacitive performance of G and pG [26, 27].

Comparison of the capacitive performance of microporous (pG) and solid films (G) reveals that microporous structures also enhance the capacitance of the electrodes. The capacitive performance of pG-PPy is higher than that of G-PPy, which further confirms that the electrode with microporous structures has a higher capacitance than the solid one even with the existence of PPy coatings. The reason might be that the microporous structures break the stacking of G sheet and lead to a more expedite diffusion and migration of electrons. Note that the conductivity of pG is lower than that of G, whereas the capacitance of pG is higher than that of G. This also holds true for the case of pG-PPy and G-PPy electrodes. These results suggest that microporous structures play a more important role than conductivity in the capacitive performance to certain extents. These results give us inspiration in future design of electrodes for supercapacitors, and more attention should be paid on the micro structure design of the electrode materials.

The capacitive performance of these four electrodes are also characterized by the galvanostatic charge–discharge test (Fig. 8a), which shows that the capacitive behaviors of G, G-PPy, pG and pG-PPy has nearly linear slopes. pG-PPy and G-PPy have longer discharging time than pG and G (Fig. 8a). These results further confirm that the incorporation of PPy coating on G and pG enhance the capacitance of G-based EDLC electrodes and PPy with the pseudocapacitance performance and plays a significant role in charge storage of the as-prepared electrodes [6, 14, 28]. The internal resistance drop (IR drop) of these four electrodes is measured (Fig. 8a). G has the highest IR drop (0.3 V) and pG-PPy has the lowest (0.1 V), which indicates that less energy is wasted during the charging–discharging process of pG-PPy.

Ragone plot (Fig. 8b) also reveals that the pG-PPy electrode has the highest energy density of 16.29 μWh cm^{-2}, corresponding to a power density of 0.134 mWh cm^{-2}. However, the cycling performance tests reveal that microporous G films have a lower stability than that of solid G films (Fig. 8c). pG-PPy, retains 82.29 % of the capacitance after 1,000 charge–discharge cycles, whereas G-PPy retains 89.74 %. Similarly, pG retains only 70.75 %, whereas G retains 73.99 %. The low stability of pG-PPy and pG might be ascribed to the microporous internal structures, which have been proved to have weak mechanical property and might become unstable connection during the charging–discharging process [29].

4 Conclusions

PPy coated G films with and without microporous structures are developed by using PS sacrificial templates and the facile PPy electrochemical deposition process. The results reveal that the PPy coatings have a significant effect on G-based electrodes. PPy coated G films have higher conductivity and capacitance than uncoated ones. The results also indicate that microporous structures play an important role in the electrochemical performance of the electrode materials. The pG-PPy electrodes, which have microporous structures and PPy coatings, have the best capacitive performance among all electrodes.

References

1. Y. Mun, C. Jo, T. Hyeon, Carbon **64**, 391 (2013)
2. M.F. El Kady, R.B. Kaner, Nat. Commun. **4**, 1475 (2013)
3. H. Jiang, P.S. Lee, C. Li, Energy Environ. Sci. **6**, 41 (2013)
4. Y. Zhu, S. Murali, W. Cai, Adv. Mater. **22**, 3906 (2010)
5. X. Cao, Y. Shi, W. Shi, Small **7**, 3163 (2011)
6. F. Liu, S. Song, D. Xue, Adv. Mater. **24**, 1089 (2012)
7. G. Wang, X. Sun, F. Lu, Small **8**, 452 (2012)
8. J. Lee, S.I. Kim, J. Yoon, ACS Nano **7**, 6047 (2013)
9. J. Zhi, W. Zhao, X. Liu, Adv. Funct. Mater. **24**, 2013 (2014)
10. T. Kim, G. Jung, S. Yoo, ACS Nano **7**, 6899 (2013)
11. J. Hu, Z. Kang, F. Li, Carbon **67**, 221 (2014)
12. B.G. Choi, M. Yang, W.H. Hong, ACS Nano **6**, 4020 (2012)
13. L.L. Zhang, X. Zhao, Chem. Soc. Rev. **38**, 2520 (2009)
14. J. Zhang, X. Zhao, J. Phys. Chem. C **116**, 5420 (2012)
15. H.P. De Oliveira, S.A. Sydlik, T.M. Swager, J. Phys. Chem. C **117**, 10270 (2013)
16. H.H. Chang, C.K. Chang, Y.C. Tsai, Carbon **50**, 2331 (2012)
17. A. Liu, C. Li, H. Bai, J. Phys. Chem. C **114**, 22783 (2010)
18. W.S. Hummers Jr, R.E. Offeman, JACS **80**, 1339 (1958)
19. L. Jiang, X. Lu, X. Zheng, J. Mater. Sci.: Mater. Electron. **25**, 174 (2014)
20. S. Pei, J. Zhao, J. Du, Carbon **48**, 4466 (2010)
21. Z. Xu, Z. Li, C.M. Holt, J. Phys. Chem. Lett. **3**, 2928 (2012)
22. J. Yan, J. Liu, Z. Fan, Carbon **50**, 2179 (2012)
23. L. Jiang, Z. Fan, Nanoscale **6**, 1922 (2014)
24. S. Bose, T. Kuila, A.K. Mishra, J. Mater. Chem. **22**, 767 (2012)
25. N.P. Wickramaratne, J. Xu, M. Wang, Chem. Mater. **26**, 2820 (2014)
26. S. Bose, N.H. Kim, T. Kuila, Nanotechnology **22**, 295202 (2011)
27. Y. Liu, Y. Zhang, G. Ma, Electrochim. Acta **88**, 519 (2013)
28. P.A. Basnayaka, M.K. Ram, E.K. Stefanakos, Electrochim. Acta **92**, 376 (2013)
29. Y. He, W. Chen, X. Li, ACS Nano **7**, 174 (2012)